Supplementary Information

Operando Imaging of Photoelectrochemical Water Oxidation Enhanced by Charge Transfer Relay Across Grain Boundaries

Wei Nie[1,5], Thomas Dittrich[2], Yuying Gao[1], Ziyuan Wang[1,3,6], Dongfeng Li[1], Xiuli Wang[1], Fengtao Fan[1*], and Can Li[1,4*]

[1]State Key Laboratory of Catalysis, Dalian Institute of Chemical Physics, Chinese Academy of Sciences, Dalian National Laboratory for Clean Energy, Dalian 116023, China

[2]Helmholtz Zentrum Berlin für Materialien und Energie GmbH, Institut für Si-Photovoltaik, Schwarzschildstr. 8, D-12489 Berlin, Germany

[3]College of Chemistry and Chemical Engineering, Xiamen University, Xiamen 361005, China

[4]University of Chinese Academy of Sciences, Beijing 100049, China.

Present address:

[5]Helmholtz Young Investigator Group Nanoscale Operando CO_2 Photo-Electrocatalysis, Helmholtz-Zentrum Berlin für Materialien und Energie GmbH, 14109 Berlin, Germany; Department of Interface Science, Fritz Haber Institute of the Max Planck Society, 14195 Berlin, Germany

[6]Department of Chemistry and Biochemistry, Queens College, Flushing, New York 11367, United States

*Corresponding author information: canli@dicp.ac.cn, ftfan@dicp.ac.cn

Quantitation of surface hole concentration using probe molecules

The probe molecule reaction selected for this study was the oxidation of $[Fe(CN)_6]^{4-}$, used to map surface hole sites and quantify surface hole concentration. This reaction proceeds via outer-sphere electron transfer, meaning the probe does not strongly interact with the electrode surface, and electron transfer occurs without bond breaking or formation. Consequently, introducing the redox species into the electrolyte does not affect the flatband potential of the $BiVO_4$ photoelectrode. The probe concentration was set at 10 mM in a 0.1 M potassium phosphate buffer. Photocurrent measurements were carried out using a nanoelectrode-based probe positioned 30 nm above the $BiVO_4$ surface to detect the reaction product, with the net photocurrent calculated by subtracting the dark current. The increased photocurrent on the nanoelectrode, sensing the amount of the generated product molecule, titrates the concentration of surface hole density according to the first-order redox reaction: $[Fe(CN)_6]^{4-} + h^+ = [Fe(CN)_6]^{3-}$. The effective area where the nanotip can collect the product molecules is determined to be ~76 nm due to the diffusion effect of the redox molecules in aqueous solution[1,2,3,4].

Kinetic model of carrier dynamics

The kinetic model of carrier dynamics to describe the transient SPV values applied here is based on the Poisson and continuity equations. A charge neutrality was performed within the $BiVO_4$ thin film layer. The densities of trap states in the grain boundaries (N_{GBs}) and surface trap states in the grain surfaces (N_{GSs}) are taken into consideration. Due to a net-charge balance, we have:

$$\Delta p(x,t) - n_{GBs,e} - n_{GSs,e} = \Delta n(x,t) - n_{GBs,h} - n_{GSs,h}$$

where $\Delta p(x,t)$ is the excess density of photogenerated holes, $\Delta n(x,t)$ is the excess density of photogenerated electrons, $n_{GBs,e}$ is the electron density in trap states in GBs, $n_{GBs,h}$ is the hole

density in trap states in GBs, $n_{GSs,e}$ is the electron density in trap states in GSs, and $n_{GSs,h}$ is the electron density in trap states in GSs. The charge separation distance is assumed to be the $BiVO_4$ layer thickness, L. The density of photogenerated free carries at t = 0 is setting by:

$$\Delta p(x,0) = \Delta n(x,0)$$

The rate equations for excess photogenerated holes and electron contains the transfer and back transfer rate constants for holes and electrons in GBs and GSs are listed below:

$$\frac{\Delta p(t)}{\Delta t} = -K_h p(t) + K_{hb} p_{FTO} - C_b(p(t)n(t) - {n_i}^2) - p(t)\sigma_{GBs,h} v_h n_{GBs,e}$$
$$- p(t)\sigma_{GSh} v_h n_{GSs,e}$$

$$\frac{\Delta n(t)}{\Delta t} = -K_e n(t) + K_{hb} n_{FTO} - C_b(p(t)n(t) - {n_i}^2) - n(t)\sigma_{GBs,e} v_e\left(N_{GBs} - n_{GBs,e}\right)$$
$$- n(t)\sigma_{GSs,e} v_e\left(N_{GSs} - n_{GSs,e}\right) + \frac{n_{GSs,e}}{\tau_{GSs,e}}$$

$$\frac{\Delta p_{FTO}}{\Delta t} = -K_h p(t) - K_{hb} p_{FTO}$$

$$\frac{\Delta n_{FTO}}{\Delta t} = -K_e n(t) - K_{eb} n_{FTO}$$

$$\frac{\Delta n_{GBs,e}}{\Delta t} = n(t)\sigma_{GBs,e} v_e\left(N_{GBs} - n_{GBs,e}\right) - p(t)\sigma_{GBs,h} v_h n_{GBs,e}$$

$$\frac{\Delta n_{GSs,e}}{\Delta t} = n(t)\sigma_{GSs,e} v_e\left(N_{GSs} - n_{GSs,e}\right) - -p(t)\sigma_{GSh} v_h n_{GSs,e} - \frac{n_{GSs,e}}{\tau_{GSs,e}}$$

where K_h, K_e and K_{hb}, K_{eb} are the transfer rates and back transfer rate constants of holes and electrons, respectively; C_b is the radiative recombination constant in $BiVO_4$; n_i is the density of intrinsic charge carriers in $BiVO_4$ film; $\sigma_{GBs,h}$, $\sigma_{GSs,h}$, $\sigma_{GBs,e}$, $\sigma_{GSs,e}$ is the capture cross sections for holes and electrons trapped in GBs and GSs, respectively; v_h, v_e is the thermal velocity of holes, thermal velocity of electrons, respectively; N_{GBs}, N_{GSs} is the density of traps in GB and GS per unit volume, respectively; p_{FTO}, n_{FTO} is the hole and electron density transferred to back FTo layer, respectively; $\tau_{GSs,e}$ is the electron lifetime at interface traps in

GS. To describe the SPV amplitude, a net-charge balance was performed within the $BiVO_4$ film according to charge neutrality. By resolving the excess density of holes and electrons, we will have SPV in the following:

$$SPV(t) = L * (\frac{\Delta p(t) - \Delta n(t) - N_{GBs}(t)}{\varepsilon_0 \varepsilon_r})$$

where ε_0, ε_r is the dielectric constant of vacuum and the relative dielectric constant of $BiVO_4$.

Supplementary Figures

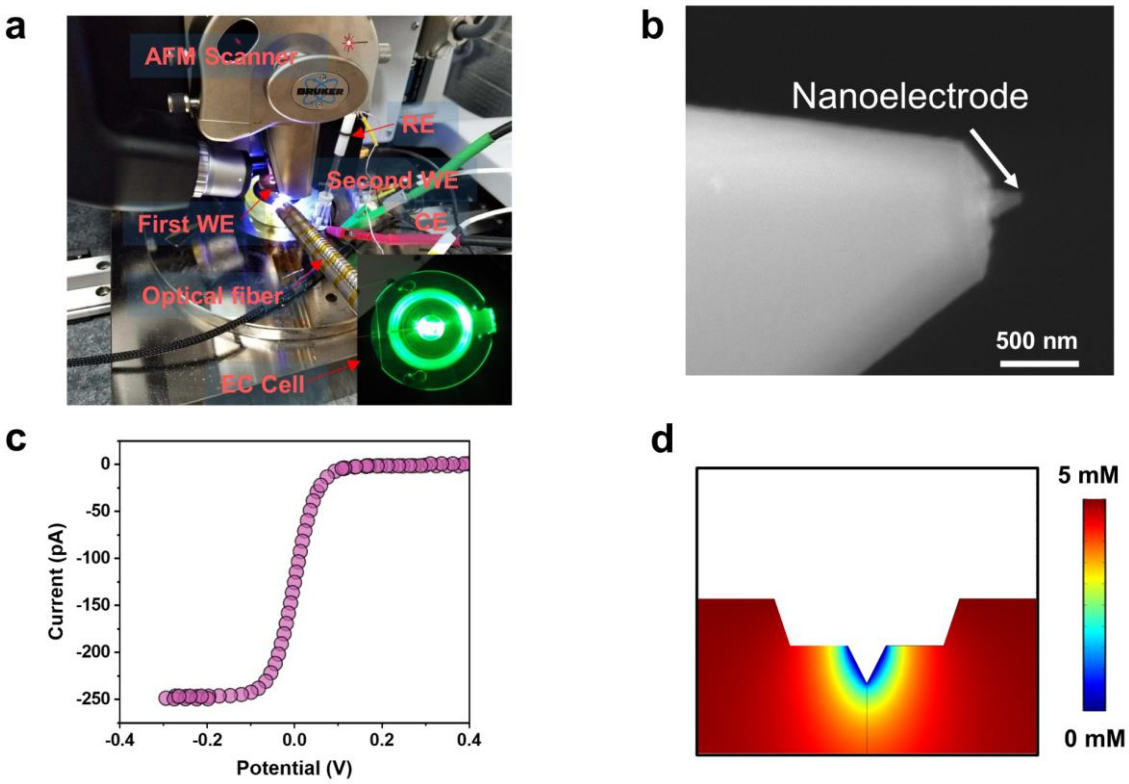

Supplementary Figure 1 a, Scanning photoelectrochemical microscopy (SPECM) measurements performed in a custom-designed electrochemical cell integrated with an optical fiber. **b,** SEM side view of the AFM-SECM cantilever and top-mounted nanoelectrode. **c,** Simulated cyclic voltammetry curve of the SPECM probe in a 5 mM redox couple solution. **d,** Simulated steady-state concentration distribution of the reactant molecules around the nanoelectrode in a 10 mM redox mediates solution.

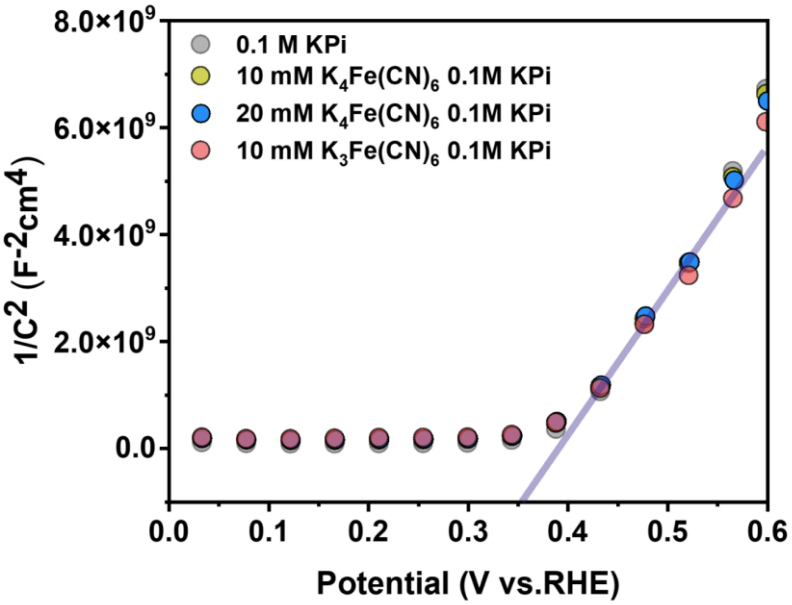

Supplementary Figure 2 Mott-Schottky plots of the $BiVO_4$ film photoelectrodes in 0.1 M KPi buffer electrolyte with and without different concentration of $K_4Fe(CN)_6$ or $K_4Fe(CN)_6$ redox mediator.

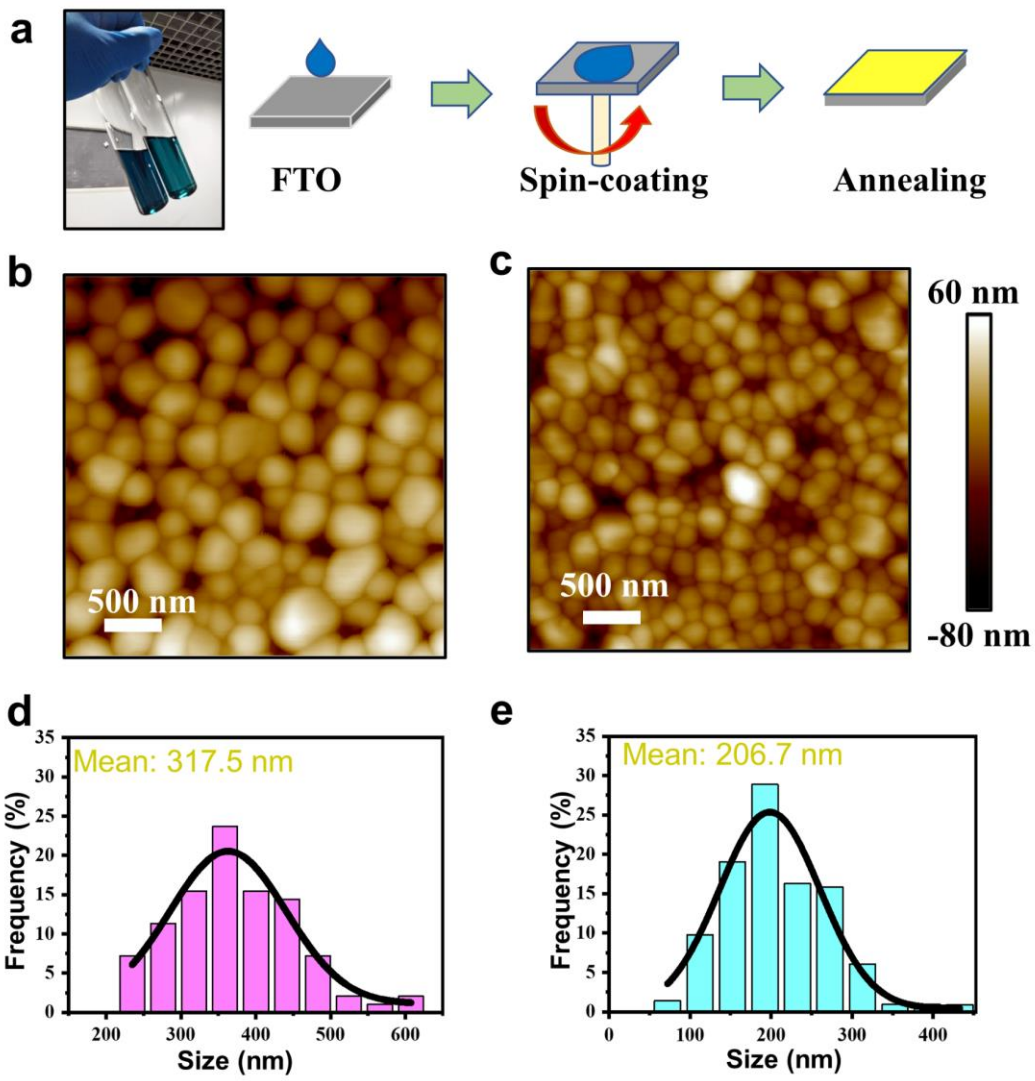

Supplementary Figure 3 a, Schematic illustration of the spin-coating process for synthesizing the $BiVO_4$ photoelectrode films. **b,** AFM image of the $BiVO_4$ film annealed at 450 °C for 10 hours. **c,** AFM image of the $BiVO_4$ film annealed at 500 °C for 5 hours. **d,** Grain size distribution histogram for the film annealed at 450 °C for 10 hours, with an average grain size of 317.5 ± 0.5 nm. **e,** Grain size distribution histogram for the film annealed at 500 °C for 5 hours, with an average grain size of 206.7 ± 0.5 nm.

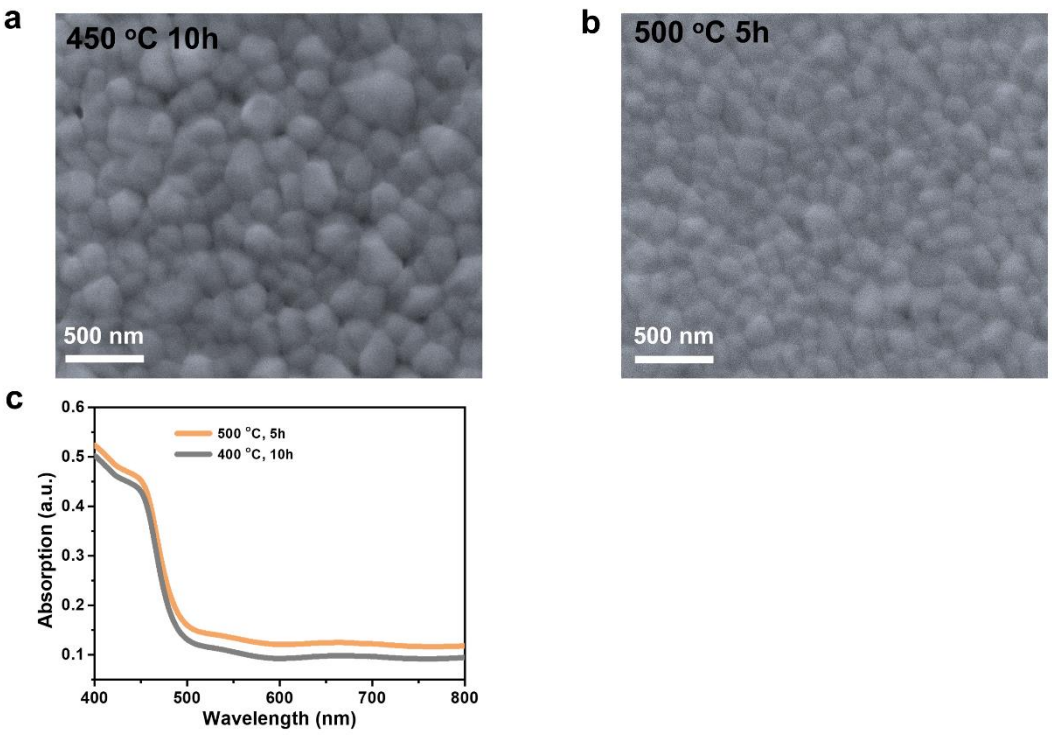

Supplementary Figure 4 a, SEM image of the $BiVO_4$ sample annealed at 450 °C for 10 hours. **b,** SEM image of the $BiVO_4$ sample annealed at 500 °C for 5 hours. **c,** UV–vis absorption spectra of the two $BiVO_4$ electrodes.

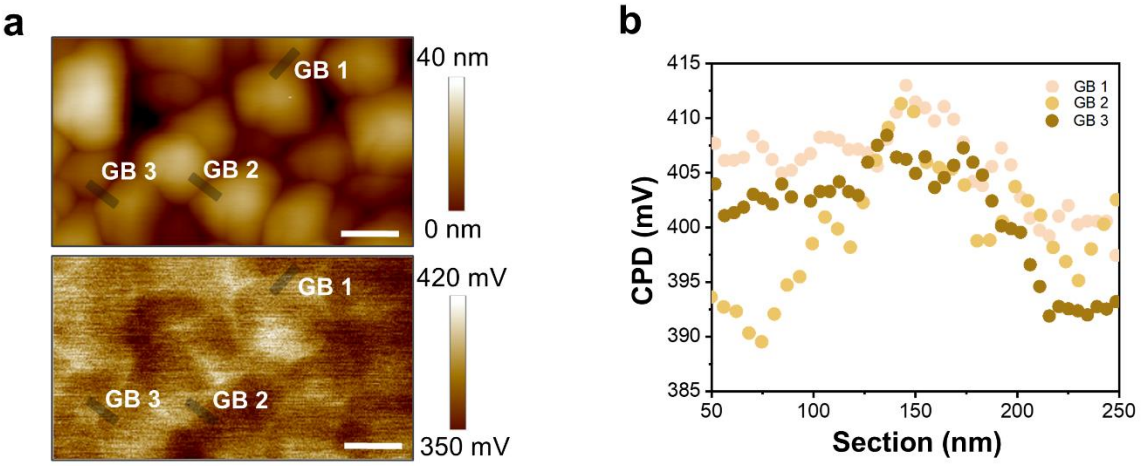

Supplementary Figure 5 a, AFM (top) and KPFM (bottom) images of $BiVO_4$ film annealed at 450 ℃ under dark conditions. Scale bars: 300 nm. The representative three GBs are marked by gray lines. **b**, CPD line profiles of the GBs extracted from the KPFM image.

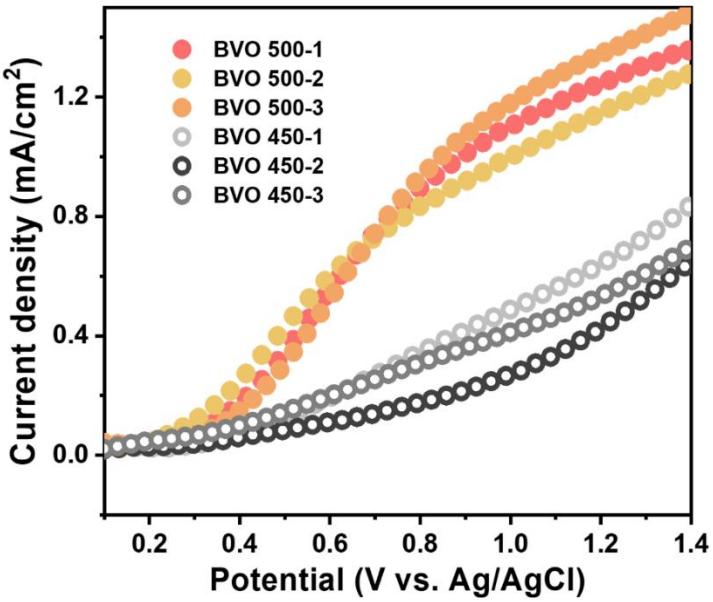

Supplementary Figure 6 Photoelectrochemical performances of the two kinds of $BiVO_4$ samples in 0.1 M KPi solution under AM 1.5 illumination. Three typical photoanode samples for each kind of $BiVO_4$ film were measured.

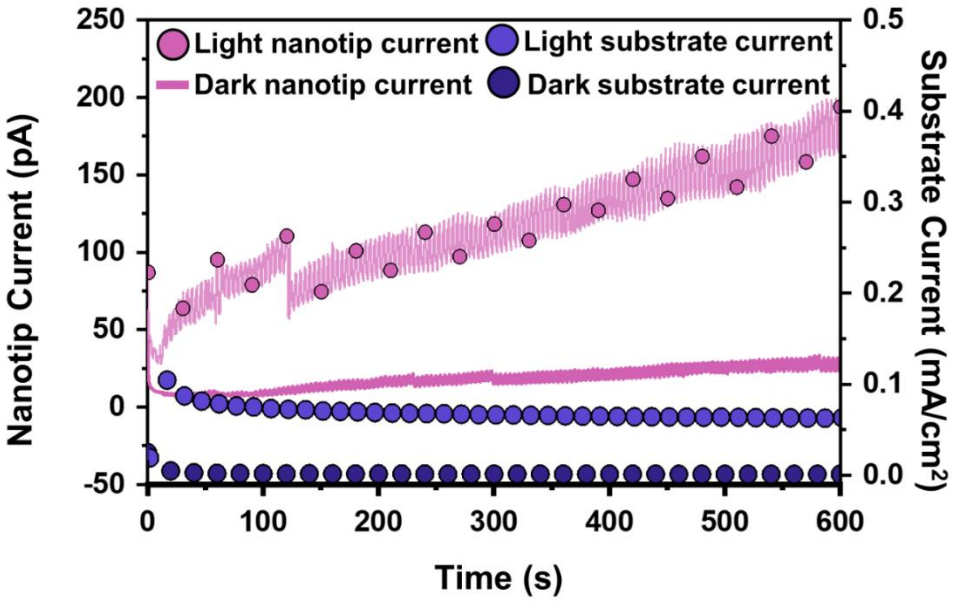

Supplementary Figure 7 Real-time nanotip and substrate currents from the SPECM image under dark and illuminated conditions for redox molecule mapping. The sample surface was biased at 0.4 V to oxidize the redox mediator, while the nanotip was held at –0.1 V to collect the generated species. The time-resolved current profiles of both the nanotip and the $BiVO_4$ photoelectrode exhibit a clear photoresponse upon illumination.

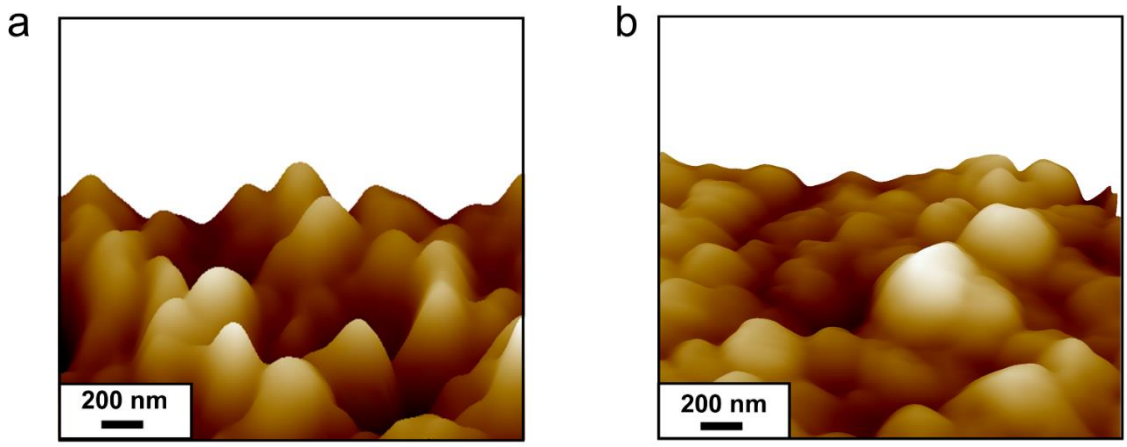

Supplementary Figure 8 Representative AFM topography images of the $BiVO_4$ film surfaces in 0.1 M KPi with/without 0.1 M $K_4[Fe(CN)_6]$, respectively in the first scan trace. **a**, Real-time topography image of the $BiVO_4$ photoanode surface annealed at 500 ℃ obtained in redox mediates electrolyte. **b**, Topography image of the $BiVO_4$ surface annealed at 500 ℃ under PEC water oxidation conditions.

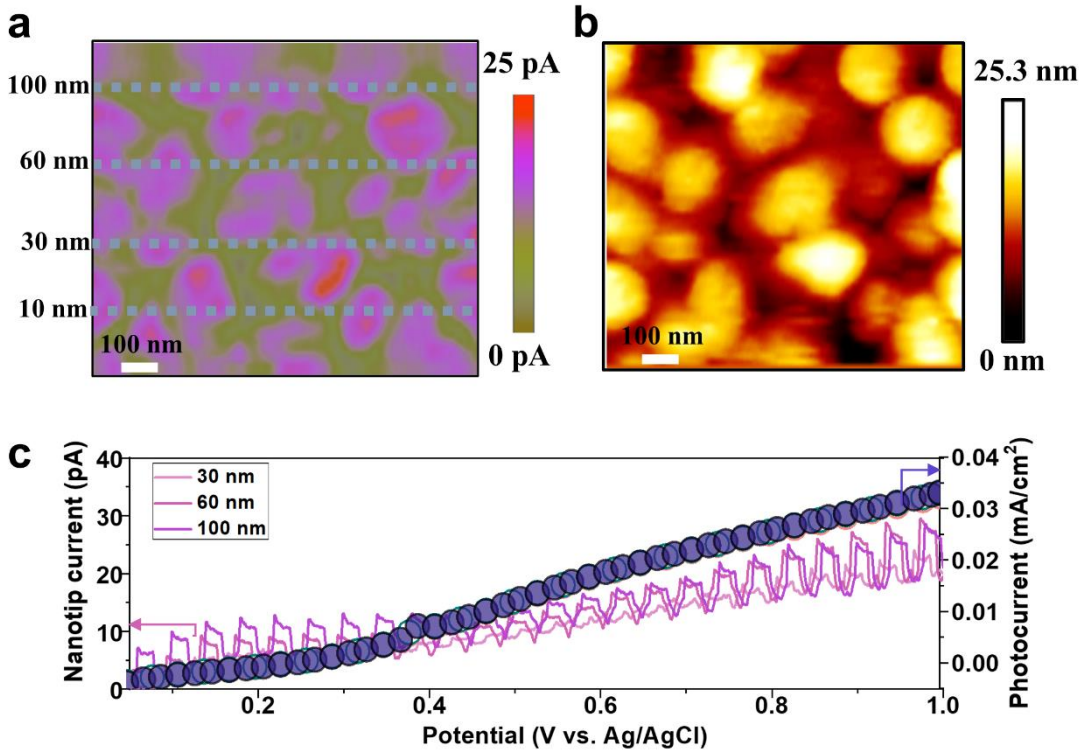

Supplementary Figure 9 a, SPECM image acquired by varying the different lift height from 10 nm to 100 nm. **b**, Corresponding AFM height image of photoanode surface. **c**, Linear sweep voltammetry of tip and substrate acquiring with different lift height. This result shows that there is no obvious spatial difference in the photocurrent and SPECM images when lifting different tip heights from 10 nm to 100 nm.

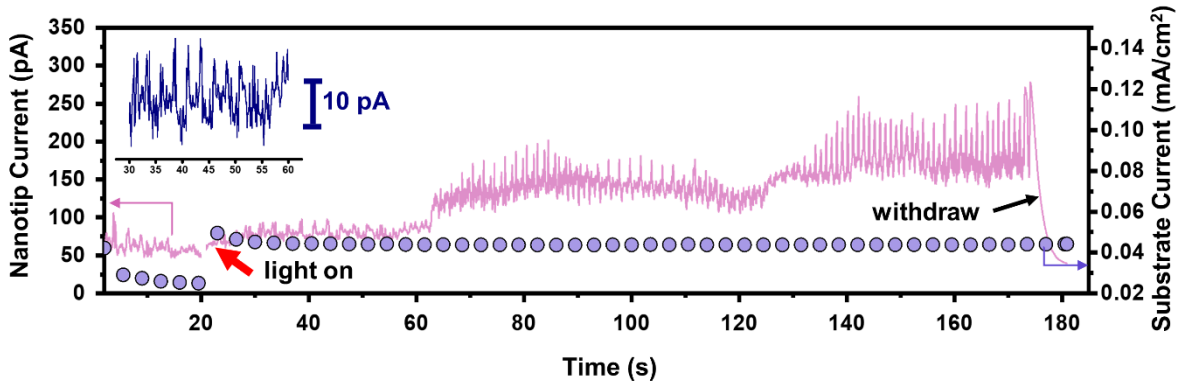

Supplementary Figure 10 Real-time nanotip current and substrate current of the SPECM imaging under dark and light condition for mapping redox molecules. The inset is the enlarged figure of the nanotip current. The real-time i-t curves demonstrate that the photocurrent of both nanotip and $BiVO_4$ photoanode increased within the sample interval (0.1 s) once the incident light was turned on. The tip current reached up to dozens of picoamperes to satisfy better signal to noise ratio when the substrate photocurrent was about only 40 $\mu A \cdot cm^{-2}$.

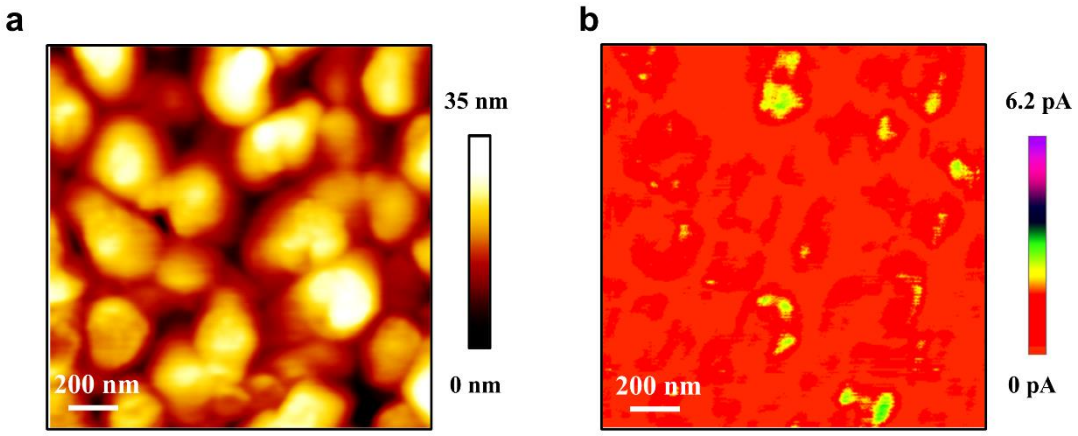

Supplementary Figure 11 a, AFM height image of $BiVO_4$ acquired under dark condition. **b**, SPECM image of the $BiVO_4$ film acquired under dark condition.

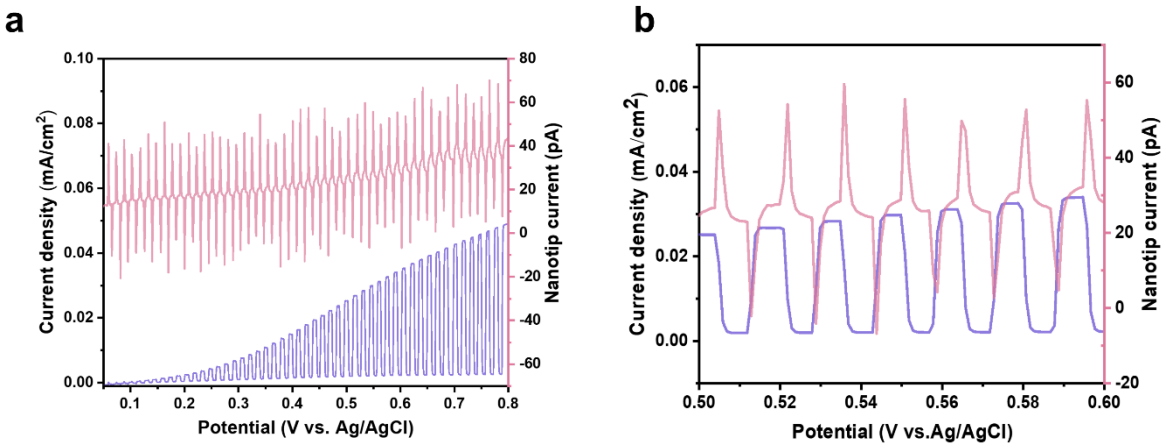

Supplementary Figure 12 a, Linear sweep voltammetry of the nanotip and $BiVO_4$ substrate under chopped light condition. **b**, Enlarged plots of the current density of the nanotip and $BiVO_4$ substrate as a function of applied potential. Chopped J-V curves were used to confirm the photocurrent response of both the photoanode and the nanotip for water oxidation process.

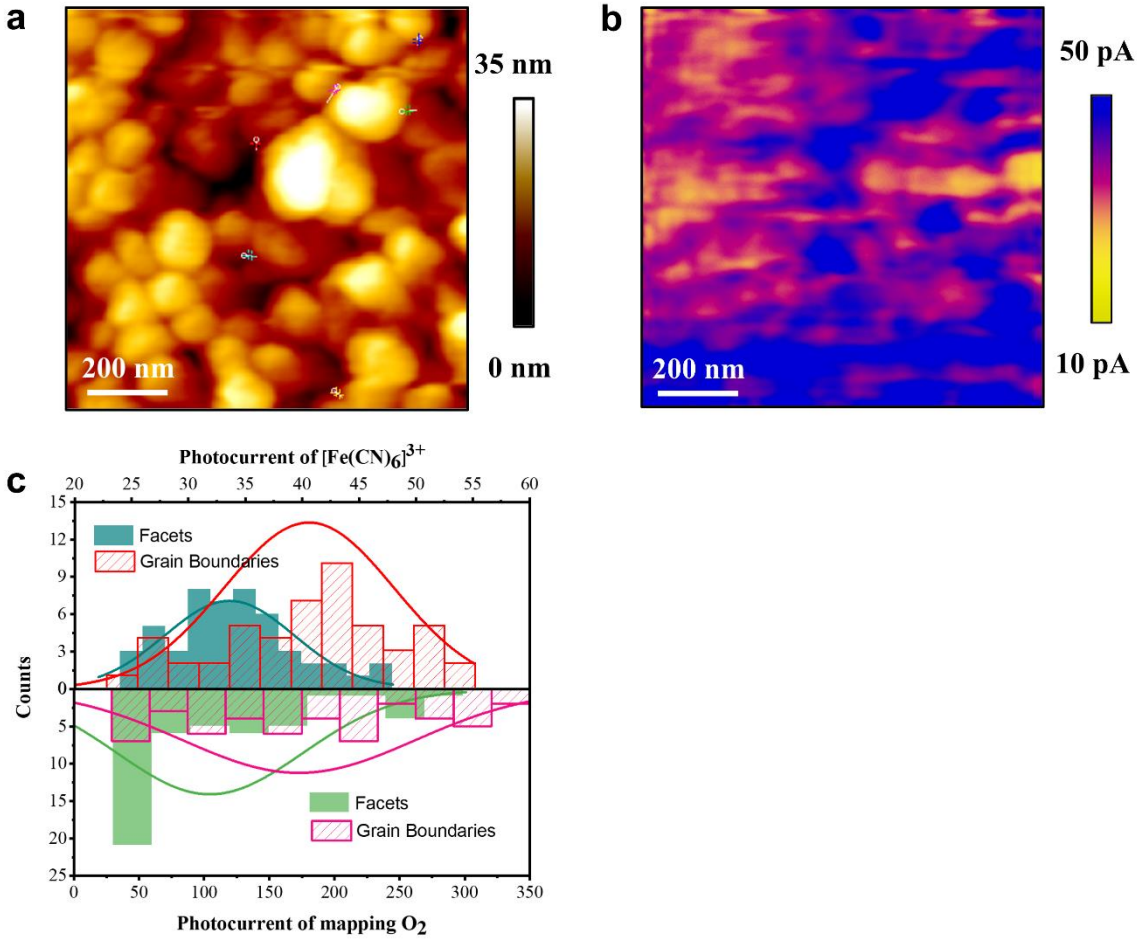

Supplementary Figure 13 a, AFM height image of the $BiVO_4$ surface when the nanotip was biased at -0.6 V (vs. Ag/AgCl) to collection O_2 molecules. **b**, 2D oxygen evolution reaction image under illumination conditions. **c**, Statistical histograms and calculation of the photocurrent of charge transfer and realistic oxygen evolution reactions on the GBs and GSs, respectively: $\frac{I_{GBs}(counts)}{I_{GBs}(counts)+I_{facets}(counts)} = \frac{9975}{9975+4200} = 70.3\%$.

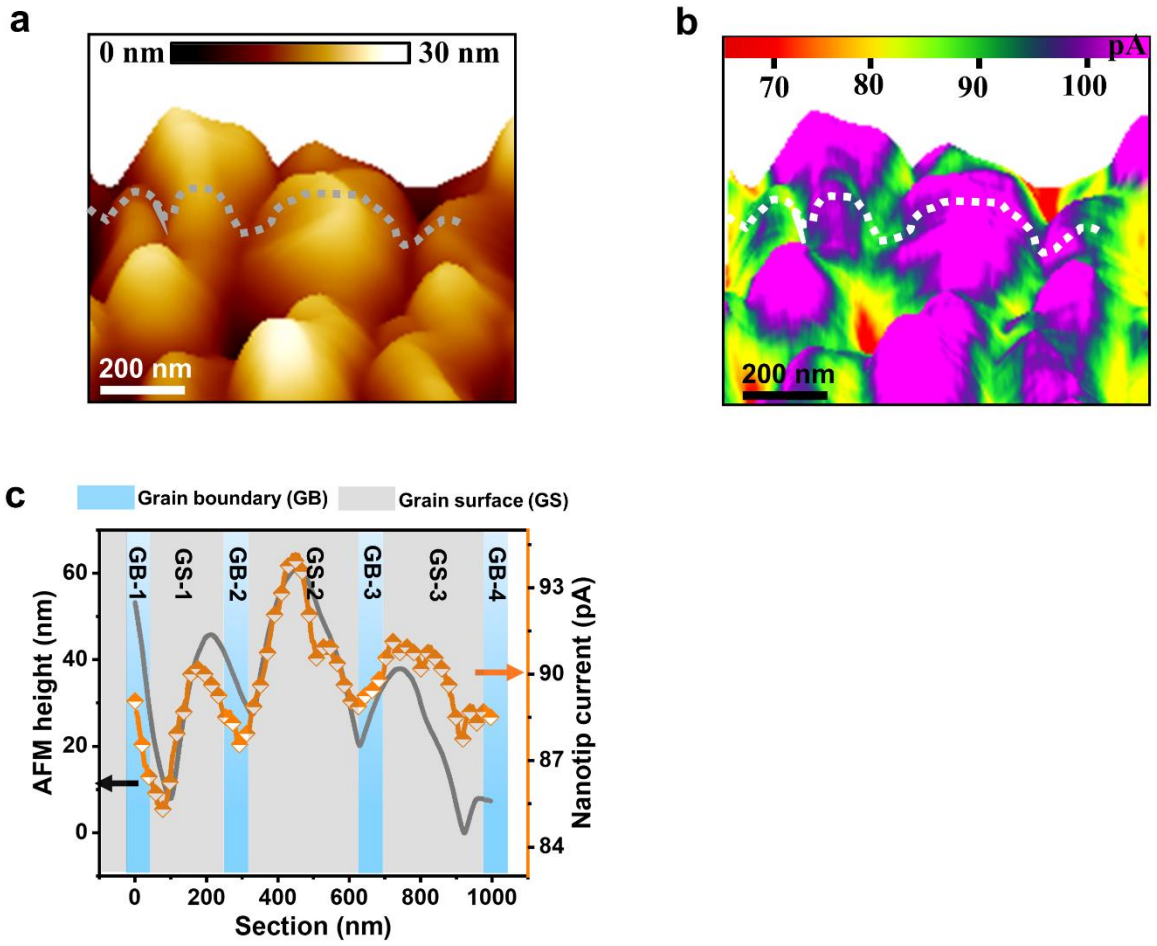

Supplementary Figure 14 a, 3D height image of the $BiVO_4$ surface with 450℃ annealing temperature and 10 hours annealing time when the nanotip was biased at -0.1 V to probe redox molecules. **b**, 3D-morphology image with overlaid charge transfer image under illumination conditions. **c**, Line profiles along the white dashed shown in **a** and **b,** simultaneously showing the morphological line profile and the corresponding charge transfer photocurrent of the nanotip.

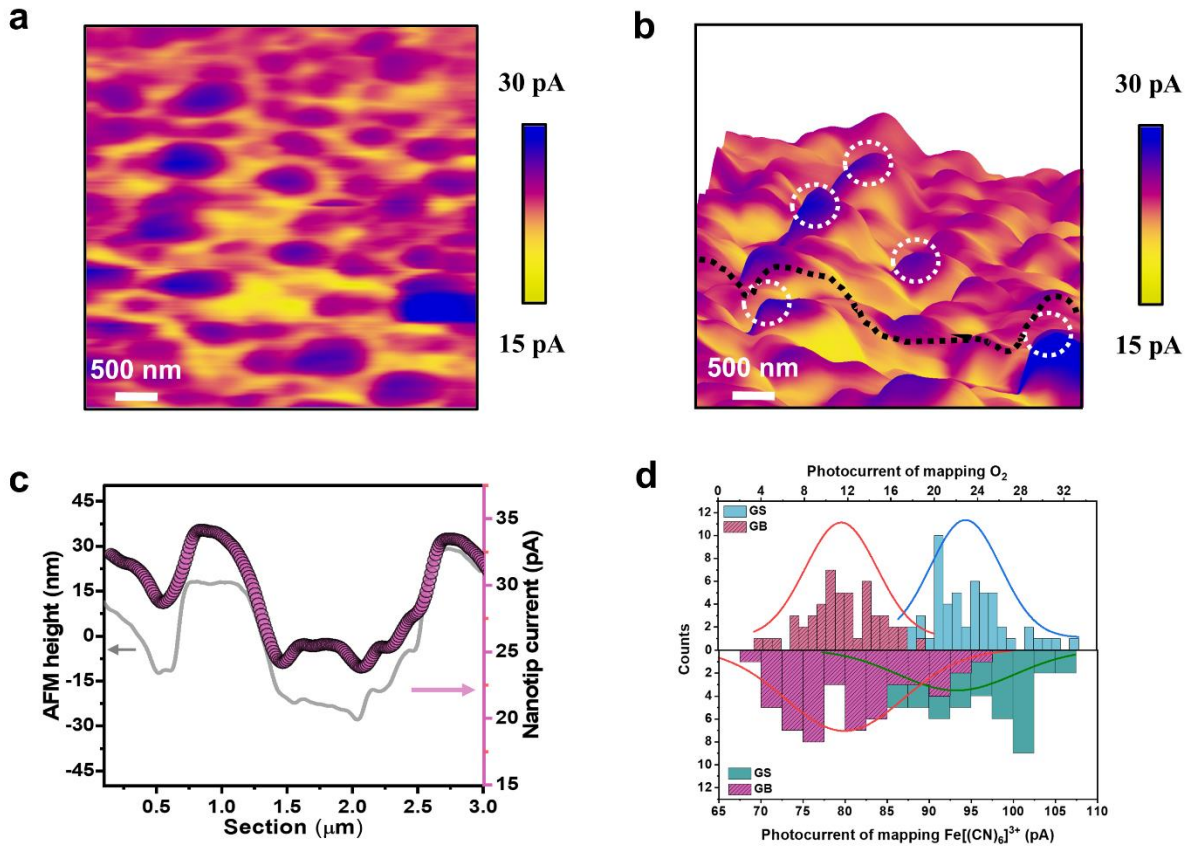

Supplementary Figure 15 a, 2D oxygen evolution reaction image of the $BiVO_4$ surface with 450℃ annealing temperature and 10 hours annealing time under a light illumination of 30 mW/cm^{-2} and a bias of +0.4 V conditions. **b**, 3D photocurrent image with overlaid topography image under illumination conditions. **c**, Line profile along the white dashed shown in **b** simultaneously showing the morphological line and the responding OER photocurrent of the nanotip. **d**, Statistical histograms of the photocurrent distributions of charge transfer and realistic oxygen evolution images on the GBs and GSs, respectively.

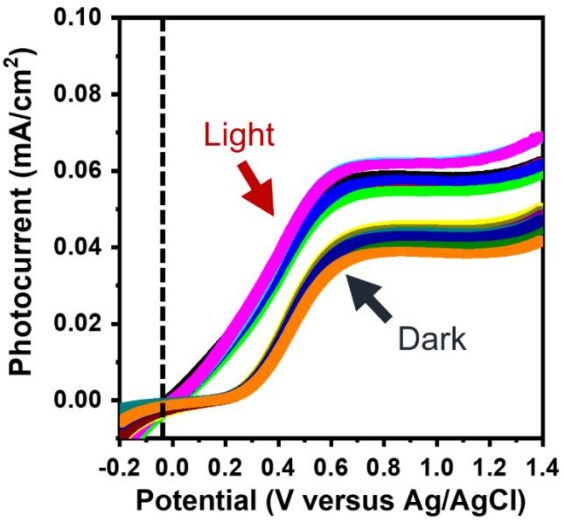

Supplementary Figure 16 a, Current-voltage (J−V) curves of the $BiVO_4$ photoanode films annealed at 500 ℃ under dark and light condition in the presence of 5 mM redox mediates.

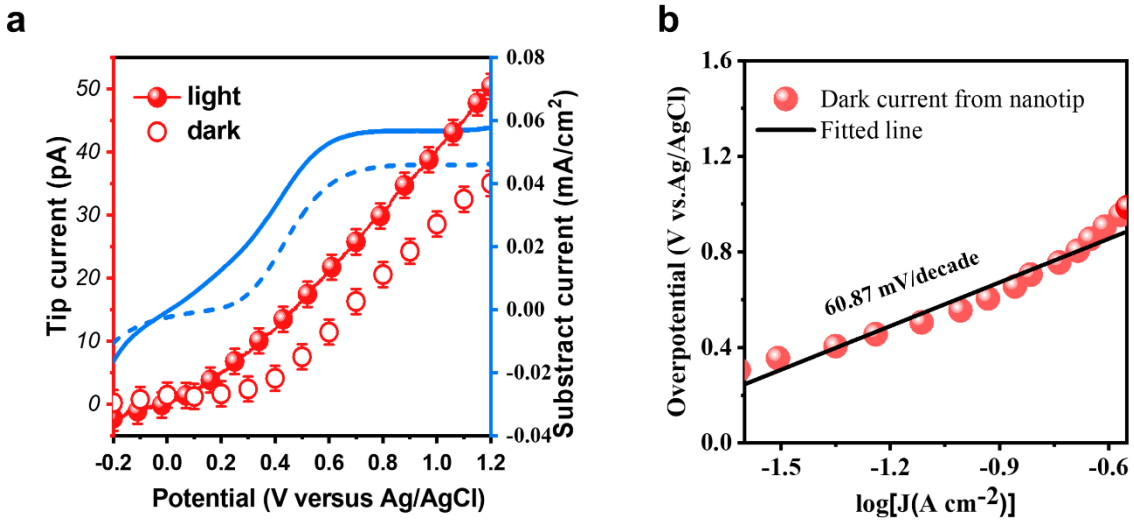

Supplementary Figure 17 a, Local current-voltage (i−E) curves of the nanotip and substrate under dark and light condition. **b**, Semilogarithmic plot versus overvoltage (Tafel curve) of the $BiVO_4$ photoelectrode.

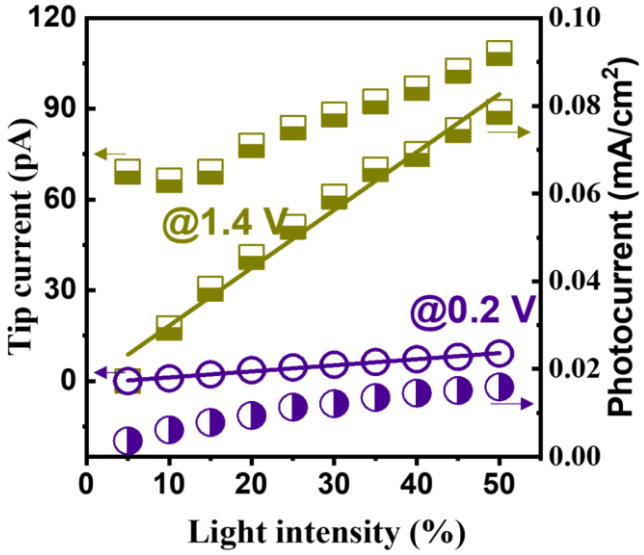

Supplementary Figure 18 Photocurrent of both the nanotip and $BiVO_4$ photoelectrode under different incident light intensity at biased voltage at 0.2 V and 1.4 V, respectively.

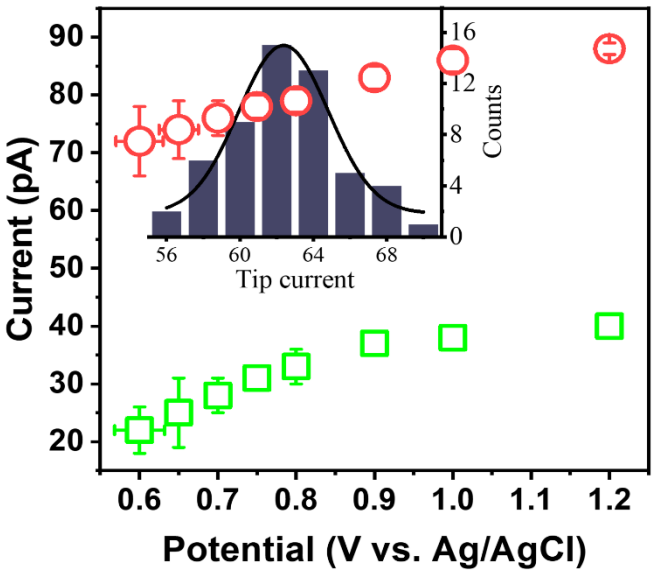

Supplementary Figure 19 Statistical current distribution analysis of photoelectrochemical water oxidation under different bias voltage.

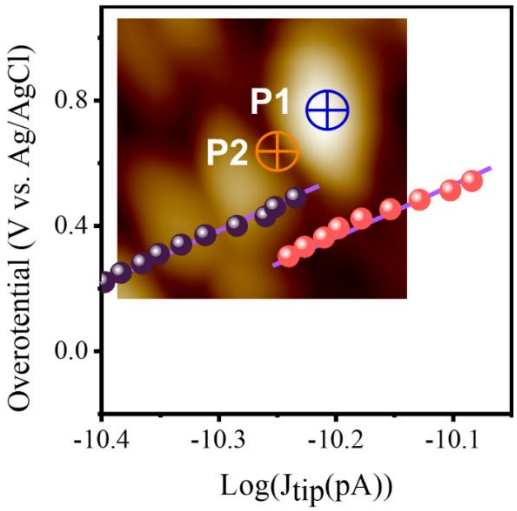

Supplementary Figure 20 Logarithmic plots of photocurrent against biased voltage at grain boundaries and facets.

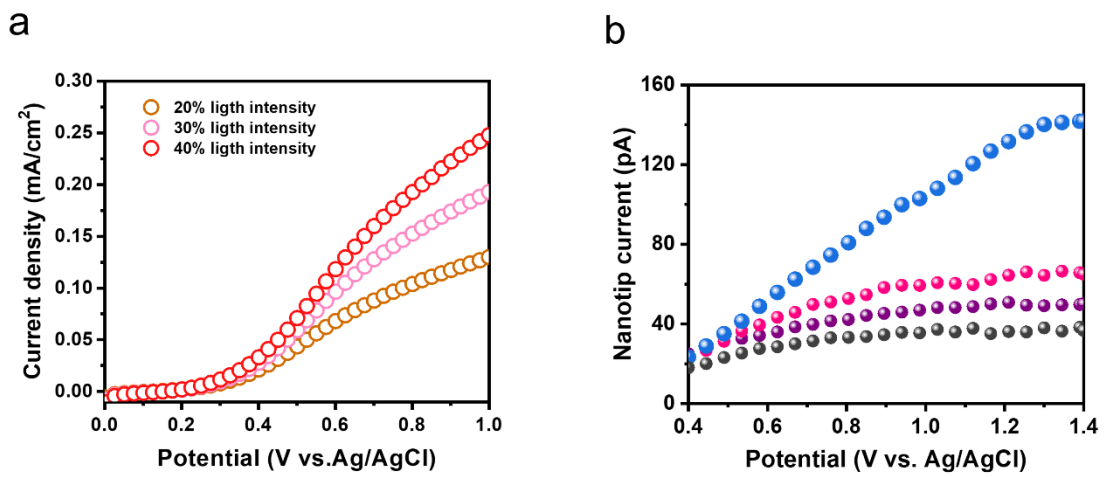

Supplementary Figure 21 a, LSV curves of $BiVO_4$ photoelectrode under different incident light intensity. **b**, LSV curves of the nanotip under different incident light intensity located 30 nm above the $BiVO_4$ surface while biased with -0.6 V for detecting O_2.

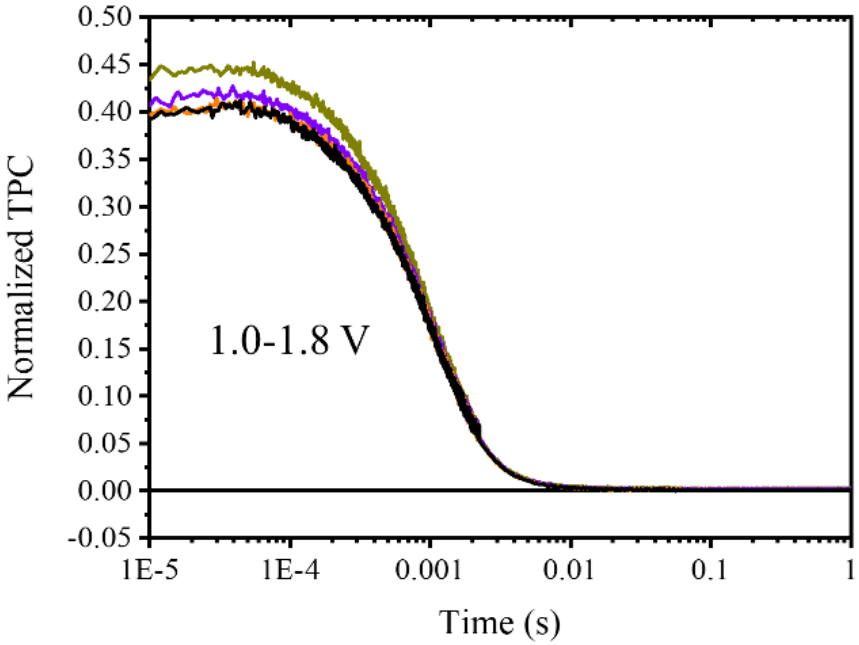

Supplementary Figure 22 Transient photocurrent (TPC) curves of $BiVO_4$ photoelectrode under biased voltage from 1.0 V to 1.8 V, showing no surface back recombination process.

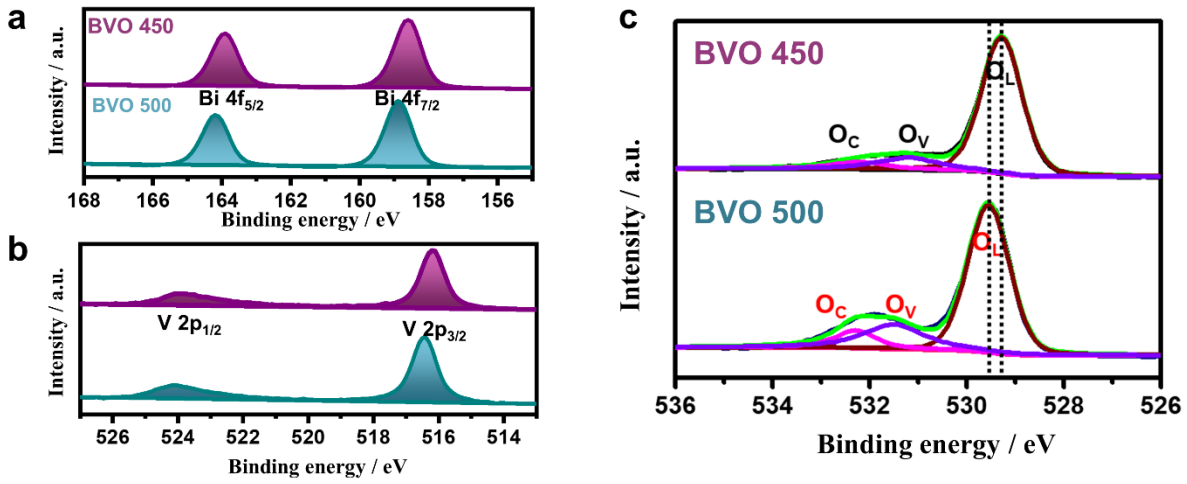

Supplementary Figure 23 a, **b**, **c**, X-ray photoelectron spectroscopy (XPS) of Bi 4f, V 2p, and O1s of the two kinds of $BiVO_4$ samples, respectively.

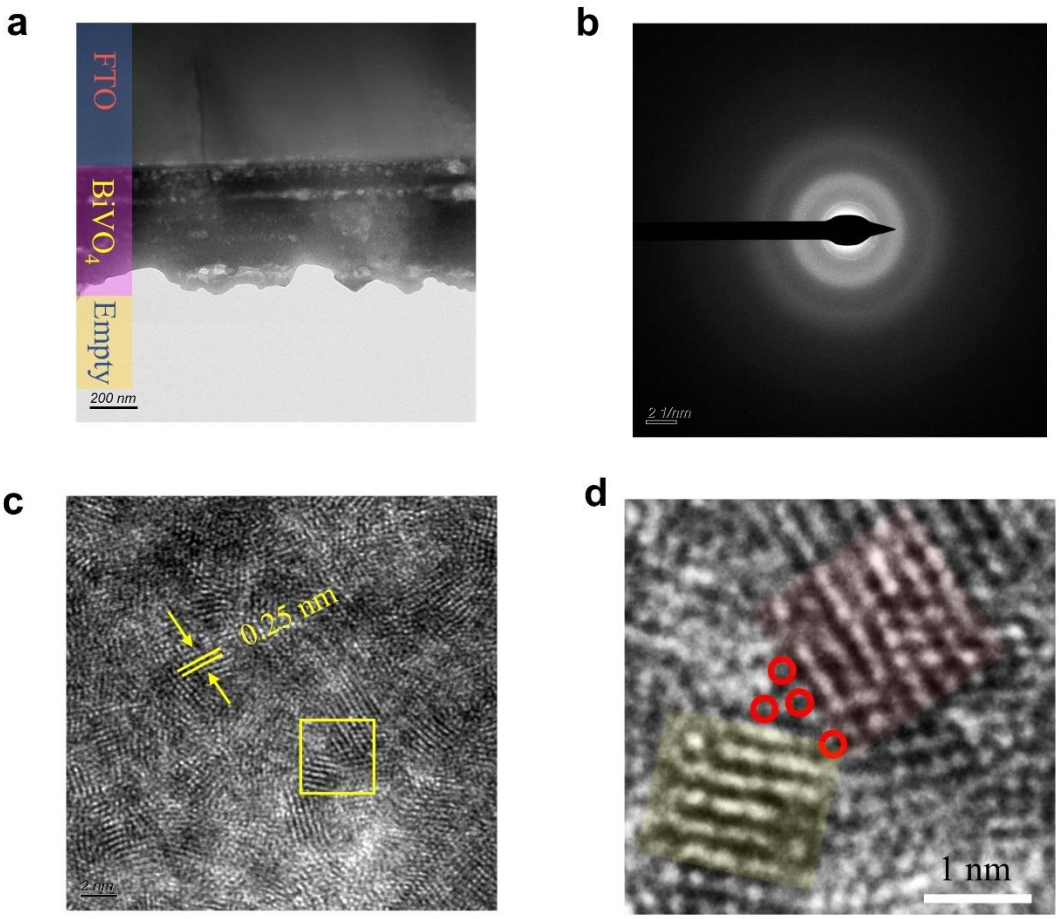

Supplementary Figure 24 a, High-resolution transmission electron microscopy (HRTEM) image of the specimen cross-section, showing the $BiVO_4$ layer annealed at 500 °C coated on fluorine-doped tin oxide (FTO) glass. **b,** Selected area electron diffraction (SAED) pattern of the polycrystalline $BiVO_4$ film. **c,** HRTEM image of the $BiVO_4$ photoanode cross-section. **d,** Magnified HRTEM view of the yellow boxed region in **c**.

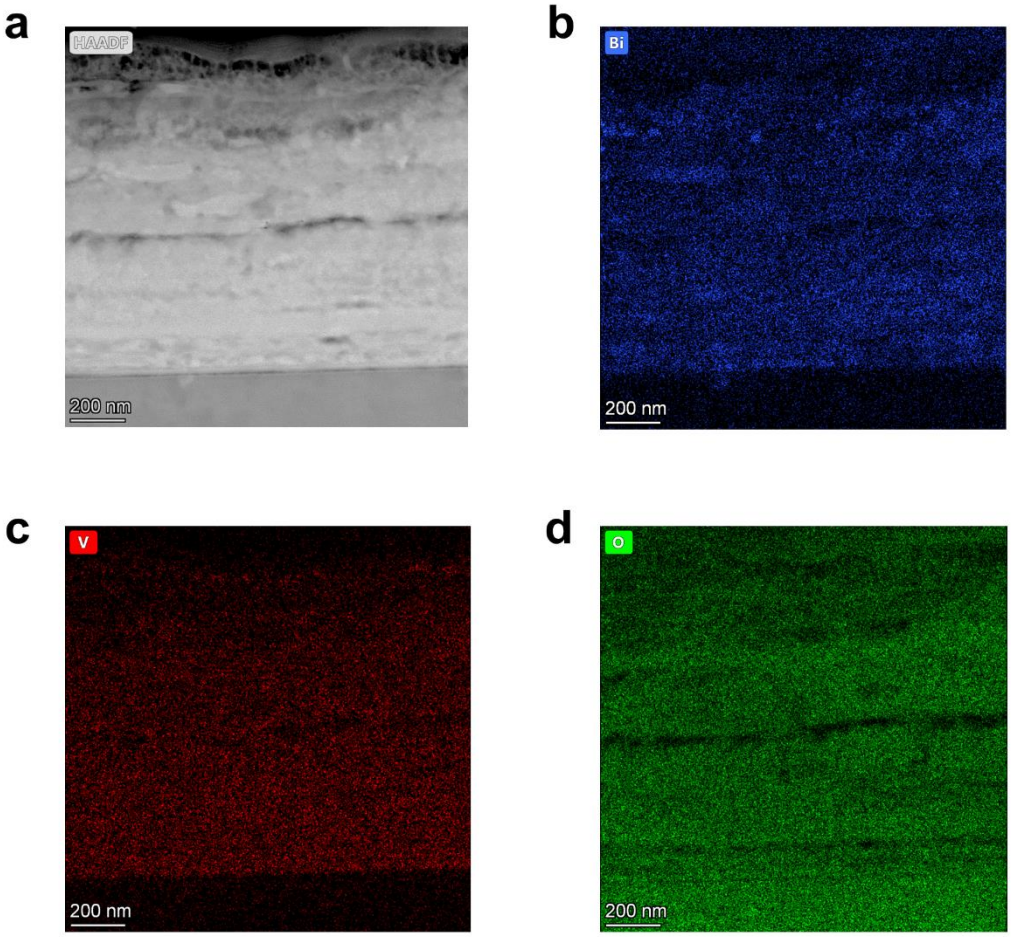

Supplementary Figure 25 a, High-angle annular dark-field scanning transmission electron microscopy (HAADF-STEM) using the same cross-sectional specimen of polycrystalline $BiVO_4$ films. **b**, **c**, **d**, Element's mapping of Bi, V, O elemental of a vertical cross-section, respectively.

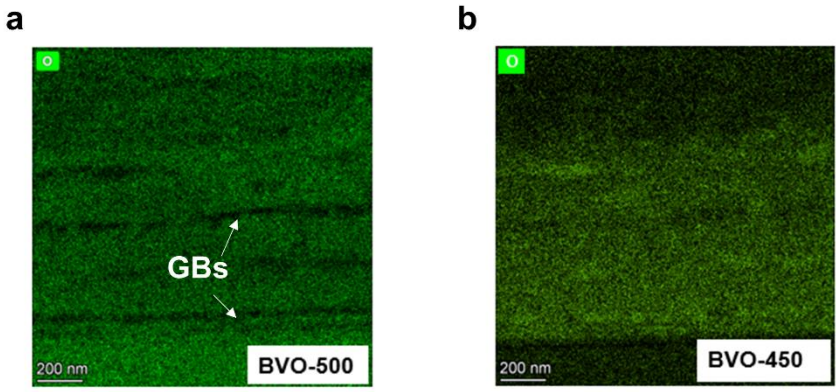

Supplementary Figure 26 a, b Cross sectional O element distributions of the $BiVO_4$ film annealed at 500 ℃ and 450℃, respectively.

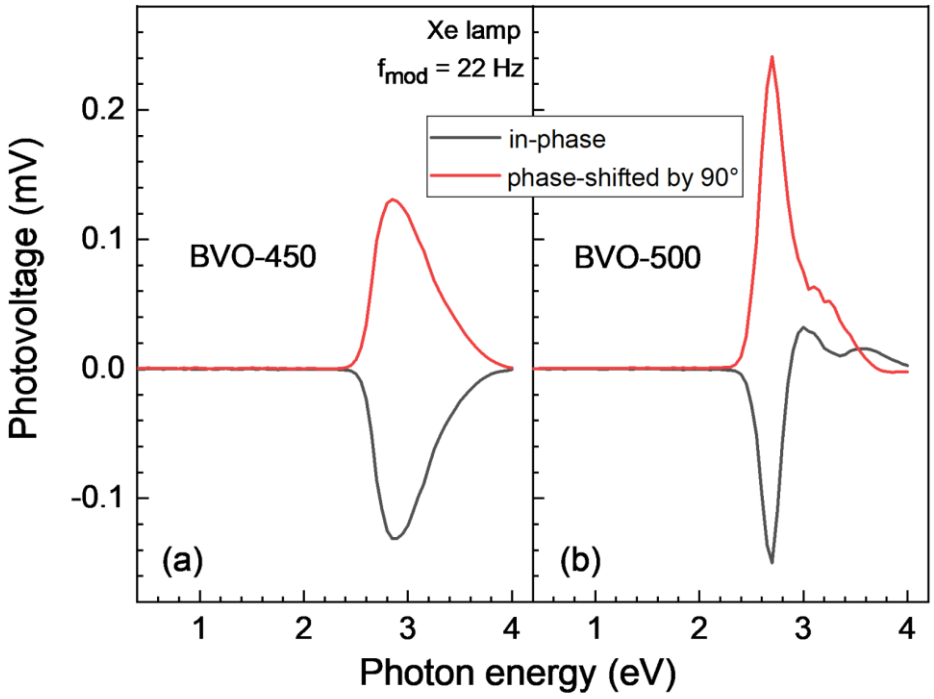

Supplementary Figure 27 Modulated surface photovoltage spectroscopy of the $BiVO_4$ films annealed at 500 ℃ and 450 ℃, respectively.

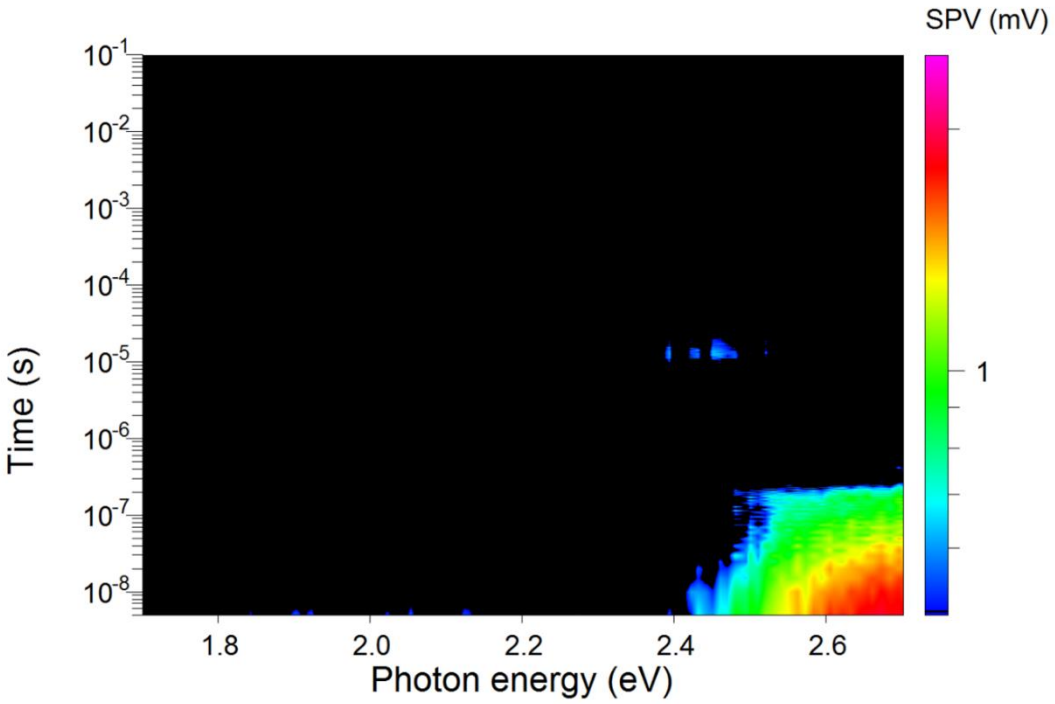

Supplementary Figure 28 2D pseudocolor plot of transient photovoltage spectrum (TPV) of $BiVO_4$ electrodes annealed at 450 ℃.

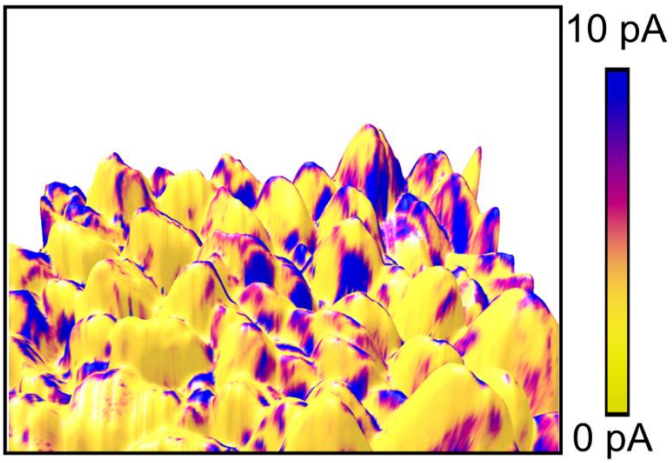

Supplementary Figure 29 Pc-AFM image with overlaid 3D morphology image of $BiVO_4$ film annealed at 500 ℃

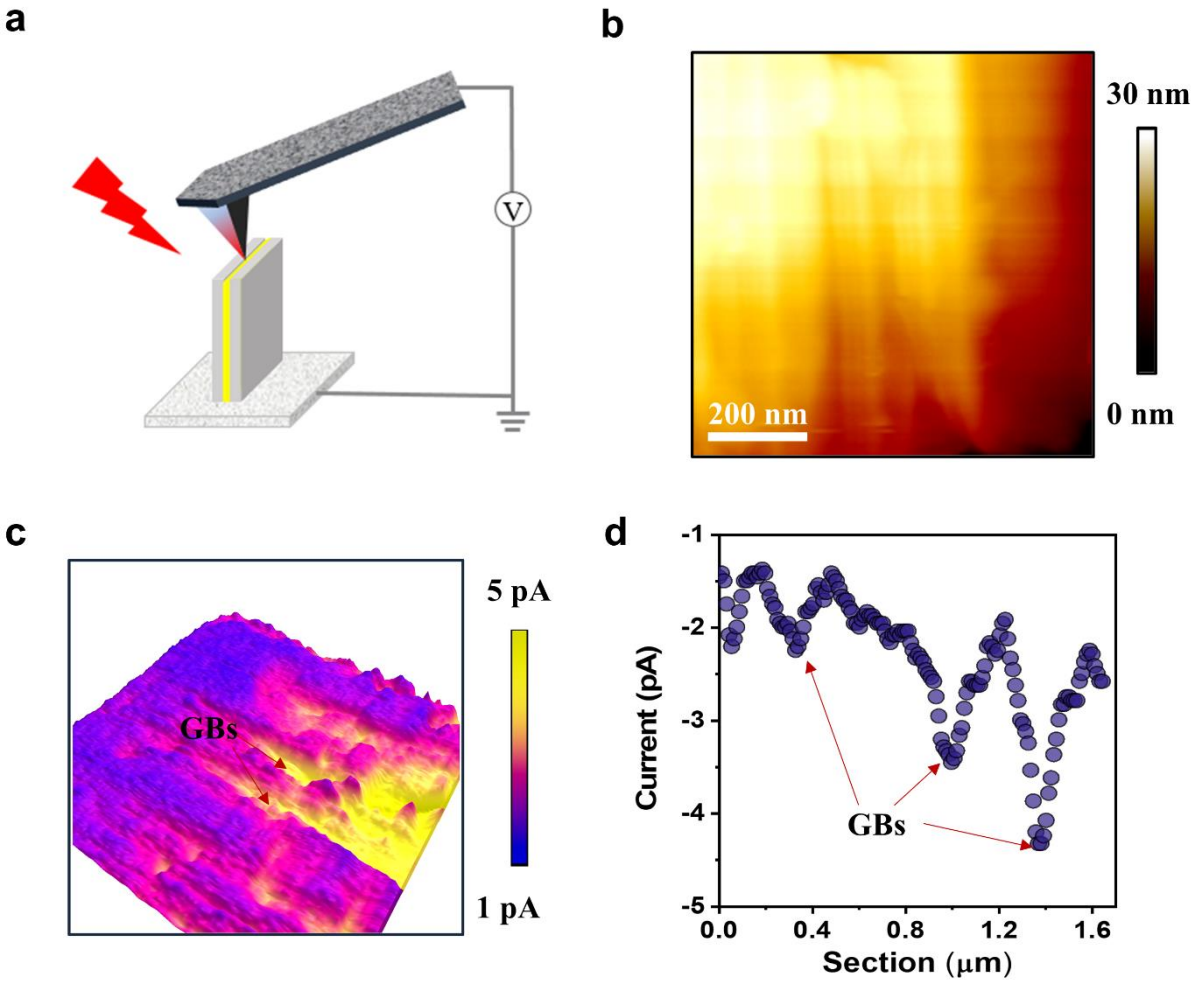

Supplementary Figure 30 a, Schematic of the pc-AFM measurement on the cross-section of the $BiVO_4$ electrodes annealed at 500 ℃. **b,** AFM morphology image of the cross-section of the $BiVO_4$ electrodes. **c,** Pc-AFM image with overlaid 3D morphology image of the cross-section of the $BiVO_4$ electrodes. **d,** Photocurrent line profile across the GBs and grain interior.

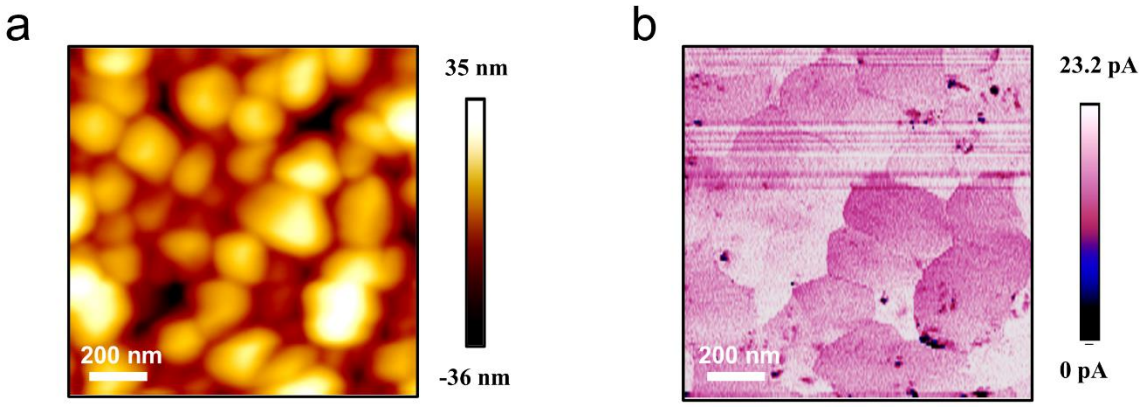

Supplementary Figure 31 a, AFM morphology image of the $BiVO_4$ electrodes annealed at 450 ℃. **b,** Corresponding pc-AFM imaging of the $BiVO_4$ electrode under 6 V, 10% light intensity.

Supplementary References

1. Nie, W. et al. Visualizing the Spatial Heterogeneity of Electron Transfer on a Metallic Nanoplate Prism. *Nano Lett.* **21**, 8901-8909 (2021).
2. Nie, W. et al. Identifying the role of the local charge density on the hydrogen evolution reaction of the photoelectrode. *J. Phys. Chem. Lett.* **12**, 10829-10836 (2021).
3. Huang, Z.Q., Poddar, R. & De Wolf, P. PeakForce scanning electrochemical microscopy with nanoelectrode probes. *Microsc. Today* **24,** 18-25 (2017).
4. Nellist, M.R. et al. Atomic force microscopy with nanoelectrode tips for high resolution electrochemical, nanoadhesion and nanoelectrical imaging. *Nanotechnology* **28,** 095711 (2017).